

Article

Development of Control Circuit for Inductive Levitation Micro-Actuators

Vitor Vlnieska^{1,‡,*} , Achim Voigt^{1,‡}, Sagar Wadhwa¹ , Jan Korvink¹ , Manfred Kohl¹ , and Kirill Poletkin^{1,2‡} 

¹ Institute of Microstructure Technology - Karlsruhe Institute of Technology, Hermann-von-Helmholtz-Platz 1, 76344 Eggenstein-Leopoldshafen, Germany; vitor.vlnieska@kit.edu

² Institute of Robotics and Computer Vision, Innopolis University, 1 Universitetskaya street, Innopolis City, 420500, Russian Federation; k.poletkin@innopolis.ru

* Correspondence: vitor.vlnieska@kit.edu;

‡ These authors contributed equally to this work.

Abstract: The control circuit for inductive levitation micro-actuators is developed in this research. The circuit performance and its electrical parameters are discussed. The developed control circuit was fabricated on a 4 layer PCB board having a size of 60×60×25 mm. It consists of a generator based on high speed Flip-Flop components and a current amplifier build on a H-bridge configuration. The circuit is able to generate AC current with squared waveform in a frequency range from 8 to 43 MHz and with a peak-to-peak amplitude up to 420 mA. To demonstrate the efficiency of developed circuit and its compatibility with a micro-actuation system, an inductive levitation micro-actuator was fabricated by using 3D micro-coil technology. The device was composed of two solenoidal coil designs, a levitation and a stabilization coil, with outer diameter being 2 and 3.8 mm respectively. A 25 μm diameter gold wire was used for fabricating the coils, with levitation coil having 20 number of turns and stabilization coil having 12 number of turns, similar to the micro-structure presented previously by our group. Using the developed control circuit, the micro-actuator was successfully excited and it demonstrated the actuation of an aluminium disc shaped micro-objects having a diameter of 2.8 and 3.2 mm and, for the first time, an aluminium square shaped having a side length of 2.8 mm at a frequency of 10 MHz. To characterize the actuation, the levitation height and the current amplitude were measured. In particular, we demonstrated that the square shaped micro-object can lift up to a height of 84 μm with current of 160 mA. The characterisation is supported by the simulation using a 3D model based on the quasi-FEM approach.

Keywords: micro-actuators; micro-systems; levitation

1. Introduction

Electromagnetic levitation micro-actuators employing remote ponderomotive forces, in order to act on a target environment or simply compensate a gravity force for holding stably a micro-object at the equilibrium without mechanical attachment, have already found wide applications and demonstrated a new generation of micro-sensors and -actuators with increased operational capabilities and overcoming the domination of friction over inertial forces at the micro-scale.

There are number of techniques, which provide the implementation of electromagnetic levitation into a micro-actuator system and can be classified according to the materials used and the sources of the force fields in two major branches: electric levitation micro-actuator (ELMA) and magnetic levitation micro-actuator (MLMA). In particular, ELMA were successfully used as linear transporters [1] and in micro-inertial sensors [2,3]. MLAM can be further split into inductive (ILMA), diamagnetic

(DLMA), superconducting micro-actuators and hybrid levitation micro-actuators (HLMA) [4], which have found applications in micro-bearings [5–7], micro-mirrors [8,9], micro-gyroscopes [10,11], micro-accelerometers [12], bistable switches [13], nano-force sensors [14], micro-transporters [15], micro-accelerators [16], micro-motors [17–19] and resonators [20].

A wide spectrum of physical principles have been utilized and successfully implemented by using different techniques for micro-fabrication. However, recently developed 3D micro-coil technology [21] together with the integration of a polymer magnetic composite material for flux concentration allows announcing inductive levitation micro-actuator systems, firstly, as systems with an established micro-fabrication process in comparison to the other levitation actuator systems and, secondly, as high-performance systems. As a results of this progress, our group demonstrated the inductive levitation actuator system with the record lowest current consumption [7] around tens of mA. This permits to avoid using standard bulky high frequency current amplifiers for exciting the ILMA and to replace them by the integrated control circuit including the signal generator and amplifier and having a size comparable with a size of micro-actuator system.

This prompted us to develop a control circuit on a 4 layer PCB board having a size of 60 x 60 x 25 mm. It consists of a generator based on high a speed Flip-Flop and a current amplifier build on a bridge configuration. The circuit is able to generate alternating current with squared waveform in the frequency range from 8 to 43 MHz and with a peak-to-peak amplitude up to 420 mA.

To demonstrate the efficiency of developed circuit, we show its successful application for excitation of an inductive levitation micro-actuator, which was fabricated using 3D micro-coil technology. The device was composed of two solenoidal coil design including levitation and stabilisation coil, having 2 mm and 3.8 mm in diameters, respectively. The levitation coil has 20 turns of a gold wire of a 25 μm diameter, while the stabilization one has 12 turns similar to the micro-structure presented previously by our group. The micro-actuator was successfully excited by the control circuit and it demonstrated the levitation of an aluminium disc shaped micro-objects having a diameter of 2.8 and 3.2 mm and, for the first time, an aluminium square shaped having a side length of 2.8 mm at a frequency of 10 MHz. To characterize the actuation, the levitation height and the current amplitude were measured. In particular, we showed that the square shaped micro-object can lift up on a height of 84 μm with rms current of 160 mA. The characterisation is supported by the simulation using a 3D model based on the quasi-FEM approach. In particular, the simulation shows that the coil design produces the maximum levitation force in order to levitate the presented square shaped proof mass (PM).

2. Development of control circuit

According to the results of the comprehensive characterization of the ILMA performance in our previous paper [22], namely, a levitation height as a function of the input parameters, i.e., the amplitude and frequency of the excitation currents, as well as the theoretical model to estimate the current versus frequency dependence for a given constant height of the disc shaped proof mass, we showed that the main advantage of using 3D microcoils in the ILMA is the possibility of increasing in the ampere-turn value as a result of an increased number of windings. This increased number of windings can be achieved in a single processing step, as opposed to, for example, the planar coils. As a consequence, the current amplitudes required to achieve similar levitation performance are reduced dramatically compared to the 2D case. However, we have also emphasized the precautions that must be taken in the case of using 3D coil structures. These are related mainly to the range of operating frequencies, which is significantly reduced to a much smaller value for the self-resonant frequency of these 3D structures compared to their 2D counterparts. Due to the reasons above discussed and the results of measurements conducted in [22], the application of 3D microcoils in ILMA requires the following electrical parameters for a voltage supplier, an excitation current, its frequency range, amplitude and waveform, which are summed up below:

- High frequency output voltage supplier from 0 to 40 Vpp;
- High frequency current (maximum peak to peak) from 0 to 400 mA;

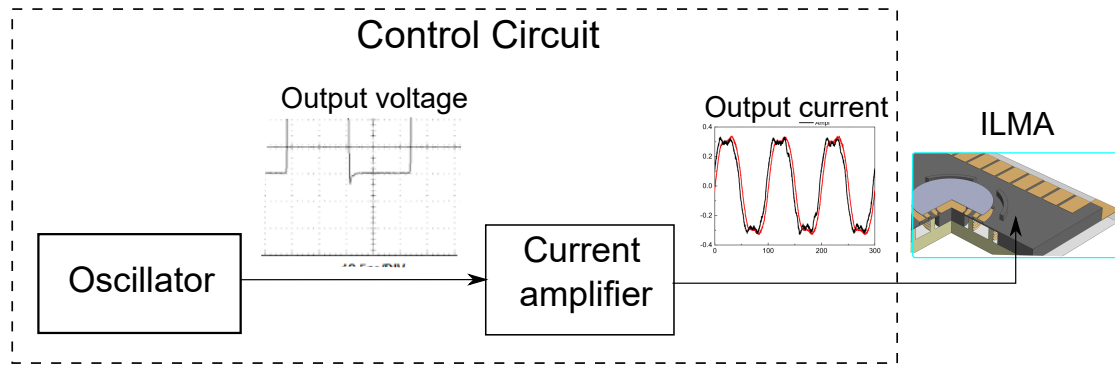


Figure 1. Schematic of the main functional elements of the control circuit.

- Rectangular waveform of the current;
- Frequency operation range from 8.4 to 40 MHz.

This list of electrical parameters is applied as the requirements for the development of the control circuit. The control circuit consists of two main functional elements as shown in Figure 1, which are a generator (oscillator) and a current amplifier. The generator is responsible for shaping the current waveform with corresponding frequency range and providing the input signal for current amplifier. Finally, the current amplifier delivers shaped AC current with the required electrical parameters to an ILMA device for its successful excitation. Hence, the development process of the control circuit can be split into two main parts, namely, the development of an oscillator and a current amplifier. Then both functional elements are integrated in one control circuit as shown in Figure 1.

The required peak to peak value of AC current up to 400 mA provides a relative high value, and the necessity of high frequency bandwidth with also high levitation coil impedance was the motivation for choosing the H-bridge configuration for building the current amplifier. The H-bridge configuration

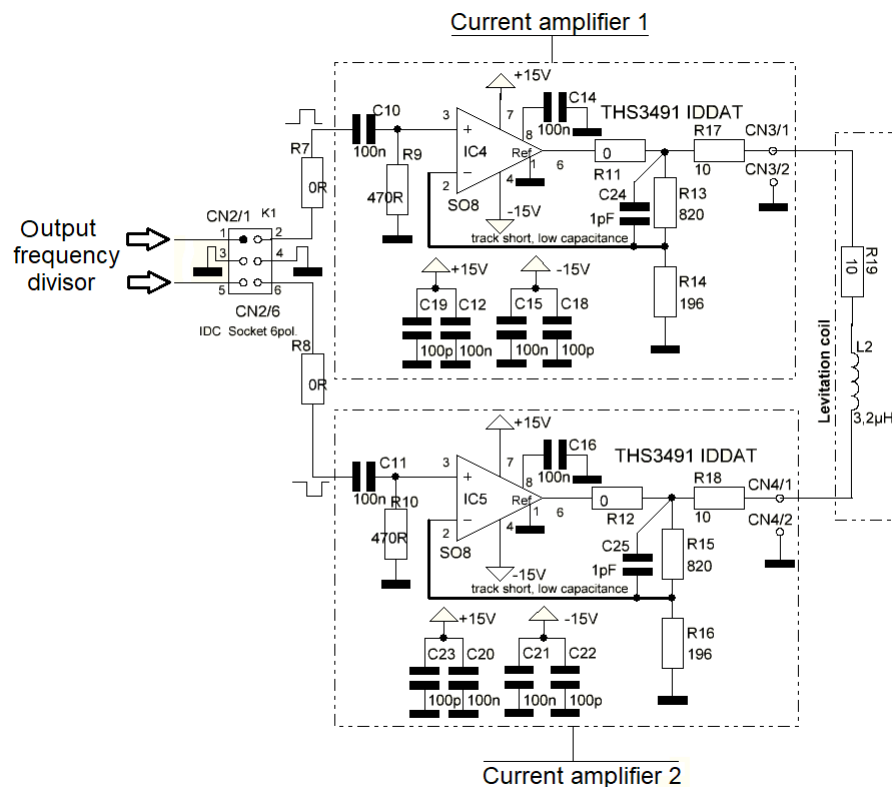


Figure 2. H-bridge configuration using two current amplifiers, at the output of the frequency divider.

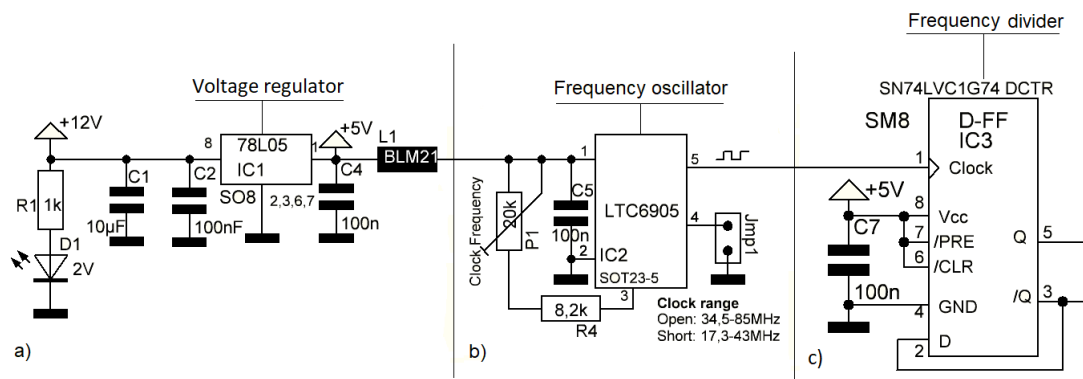


Figure 3. Electronic circuit of oscillator (implemented on a chip LTC6905 - (b)), connected to the voltage regulator (implemented on a chip LM7805 - (a)) having the voltage limit, which is up to 5.5 V. In the output of the frequency oscillator is located the frequency divider (implemented on an chip SN74LVC1G74 - (c))

avoids the usage of a transformer which its disadvantages of bandwidth limitation and enhanced input current consumption. The amplifier was accompanied with an active cooling system to avoid overheating of the electronic components. To realise the proposed configuration and to fulfil the output power and the frequency condition, two high-power output current feedback amplifiers (THS3491) developed by Texas Instruments (Austin, USA) were used. Figure 2 shows the design of electrical circuit of the current amplifier build on the H-bridge configuration by using two chips (THS3491), which are supported by double voltage suppliers of ± 15 V. The input voltage for current amplifiers is controlled by the frequency divider flip-flop (please see Figure 3, (c)), which helps providing the symmetrically signals between the output of oscillator and the inputs of the amplifiers. The output frequency given by the frequency oscillator is reduced by a factor of two.

Consequently, the oscillator must provide a frequency range more than 80 MHz. To meet this requirement, the oscillator was realized on the LTC6905 chip, which is easy to use and occupies very little board space. It requires only a single resistor to set the output frequency up to 170 MHz with a typical frequency error 0.5% or less. The designed circuit of the oscillator is shown in Figure 3. It is supplied by a single voltage supplier of 5 V. Voltage regulator (chip LM7805) helps providing

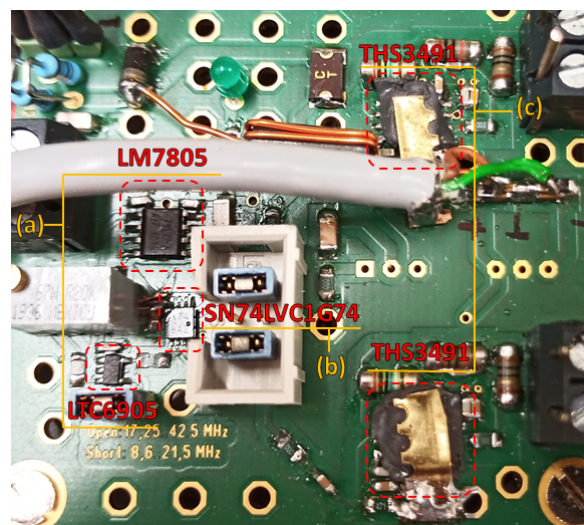


Figure 4. Control circuit built in a 4 layer PCB: the location of the voltage regulator (LM7805), and the frequency oscillator (LTC6905) is marked by (a); the location of the oscillator divisor (SN74LVC1G74) is marked by (b); the location of the two amplifiers is marked by (c).

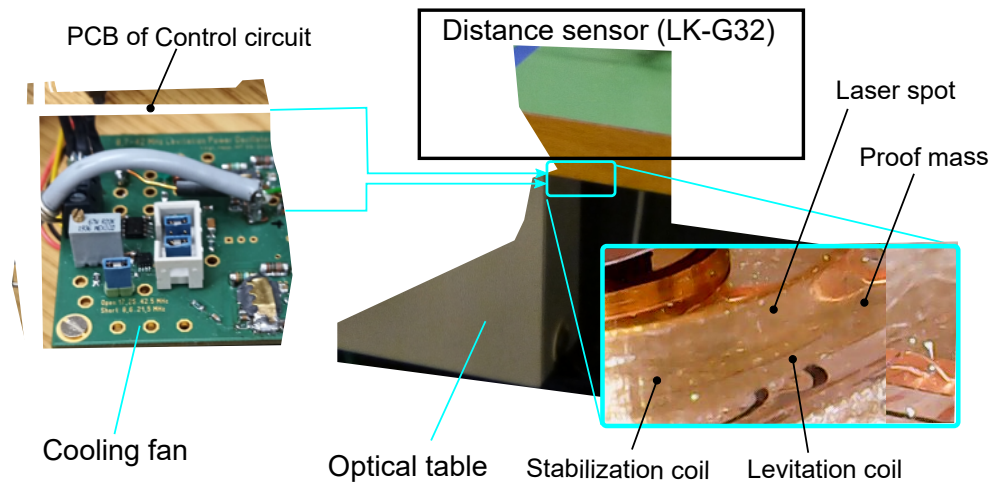


Figure 5. Experimental setup: the device is mounted on the optical table and successfully levitated the disc shaped proof mass of a 3.2 mm diameter.

the required supplying voltage. The change in the range of oscillation frequency is performed by a jumper. When the jumper is closed the frequency range is from 7.6 to 26 MHz and when it is opened, the frequency range becomes form 15 to 50 MHz. The jumper connector is located in the frequency oscillator circuit (Jmp1) as shown in Figure 3, (b)).

Finally, the proposed circuit design was fabricated on the 4 layer PCB board having a dimension of $60 \times 60 \times 25$ mm. Figure 4 shows the top view of the PCB with the location of the voltage regulator (LM7805), the frequency oscillator (LTC6905), divisor (SN74LVC1G74) and the two amplifiers (THS3491). The cooling system, which is located behind, is not visible on the Figure.

2.1. Experimental setup

In order to verify the developed control circuit and demonstrate its successful application to ILMA, we organized the following experimental setup as shown in Figure 5. The fabricated device of ILMA was mounted on the PCB board and fixed on the optical table. The device was composed of two solenoidal coil design including levitation and stabilisation coil, having 2 mm and 3.8 mm in diameters, respectively. The levitation coil has 20 turns of a gold wire of a $25 \mu\text{m}$ diameter, while the stabilization one has 12 turns similar to the micro-structure presented previously by our group [6].

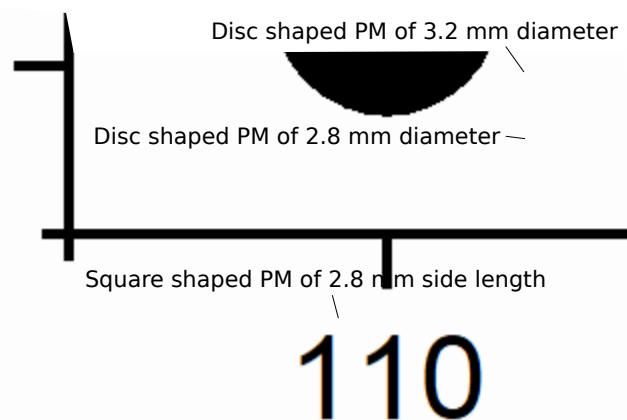


Figure 6. Measurements of the levitation height for three PMs versus the coil currents.

To control the levitation height of a levitated PM in the vertical direction, the laser sensor (LK-G32) was used. It was mounted on the optical table, above of the proof mass (PM). Then, the PCB with the developed control circuit was connected to the device as shown in Figure 5, which shows also the location of the cooling system under the circuit PCB.

For the experiment, a set of proof masses, in disc and square shapes were fabricated using an aluminium foil with the thickness ranging from $10\ \mu\text{m}$ to $15\ \mu\text{m}$. Using the described experimental setup and the developed control circuit, we were able to successfully levitate the disc shaped PM of diameters of 2.8 mm and 3.2 mm and, for the first time, square shaped PM of a side length of 2.8 mm at excitation AC frequency of 10 MHz. In particular, Figure 5 shows the levitation of the disc shaped PM of a diameter 3.2 mm at a height of $90\ \mu\text{m}$. The results of measurements of levitation heights of listed PM versus the coil current and the applied voltage are shown in Figure 6.

3. Simulation

The mechanism of stable levitation of the square shape proof mass in the framework of two coil design is similar to one as described in our previous work [23]. The induced eddy currents are distributed along the levitated proof mass in such a way that two circuits having maximum values of eddy current density can be identified. The fact will be also demonstrated by performing the simulation based on quasi-FEM model. The first circuit is corresponded to the eddy current distributed along the edge of square-shaped PM and the second circuit is defined by the levitation coil. The later one has a circular path with radius equal to the radius of the levitation coil. This mechanism can be split into two force interactions. The force interaction happens between the current in the stabilization coil and induced eddy current corresponding to the first circuit, which contributes mainly to the lateral stability of the levitated PM. While, the force interaction between the current in the levitation coil and induced eddy current corresponding the second circuit contributes mainly to the vertical and angular stability of the levitated PM.

The simulation is directed to study the levitation force and to demonstrate that the current coil design produces the maximum levitation force under the keeping the same value of the current in the coils, to levitate the square shaped PM having a side length of 2.8 mm. For such a simulation the method based on a quasi-FEM approach is applied [24,25].

3.1. Simulation of induced eddy current within the proof mass

At the beginning, the levitated micro-object is meshed by circular elements of the same radius, $R_e = 2.8025 \times 10^{-3}\ \text{m}$, as shown in Fig. 7, a value of which is defined by a number of elements,

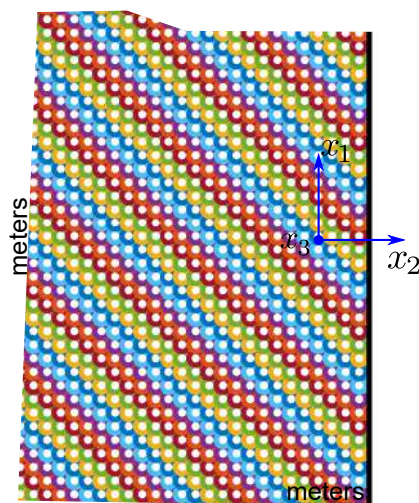


Figure 7. Square shaped proof mass of a side length of 3.4 mm is meshed by 2500 circular elements.

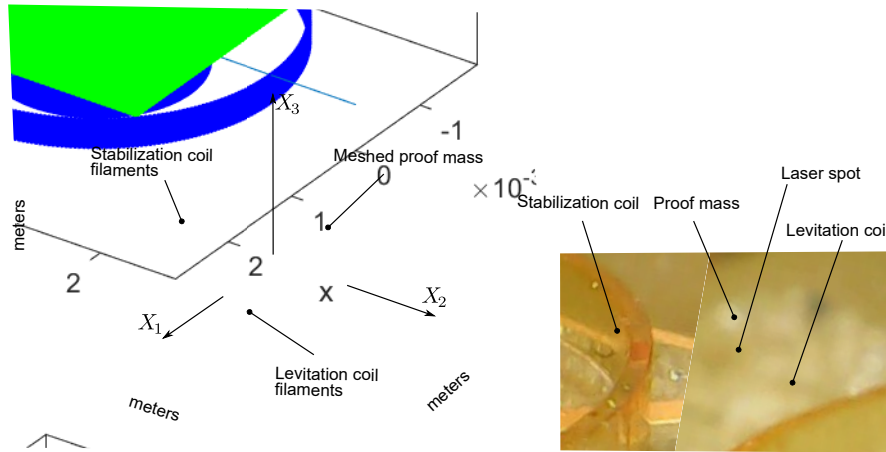


Figure 8. 3D geometrical scheme of the actuator for simulation mimicking the real prototype of actuator shown on the right side of the figure: $\{X_k\}$ ($k = 1, 2, 3$) is the fixed coordinate frame.

$n = 2500$. 3D geometry of two micro-coils is approximated by a series of circular filaments. The levitation coil is replaced by 20 circular filaments having a diameter of 2.0 mm, while the stabilization coil by 12 circular filaments with a diameter of 3.9 mm. Thus, the total number of circular filaments, N , is 32. Assigning the origin of the fixed frame $\{X_k\}$ ($k = 1, 2, 3$) to the centre of the circular filament corresponding to the first top winding of the levitation coil, the linear position of the circular filaments of levitation coil can be defined as ${}^{(j)}r_c = [0 \ 0 \ (j-1) \cdot p]^T$, ($j = 1, \dots, 20$), where p is the pitch equaling to $25 \mu\text{m}$. The same is applicable for stabilization coil, ${}^{(j)}r_c = [0 \ 0 \ (j-21) \cdot p]^T$, with the difference that the index j is varied from 21 to 32. For both coils, the Brayn angle of each circular filament is ${}^{(j)}\phi_c = [0 \ 0 \ 0]^T$, ($j = 1, \dots, 32$).

The result of meshing becomes a list of elements $\{{}^{(s)}\underline{c} = [{}^{(s)}\rho \ {}^{(s)}\phi]^T\}$ ($s = 1, \dots, n$) containing information about a radius vector and an angular orientation for each element with respect to the coordinate frame $\{x_k\}$ ($k = 1, 2, 3$). Now a matrix \underline{L} can be formed as follows

$$\underline{L} = L^o \underline{E} + \underline{M}^o, \quad (1)$$

where \underline{E} is the (2500×2500) unit matrix, \underline{M}^o is the (2500×2500) -symmetric hollow matrix whose elements are L_{ks}^o ($k \neq s$). The self-inductance of the circular element is calculated by the known formula for a circular ring of circular cross-section

$$L^o = \mu_0 R_e \left[\ln 8/\varepsilon - 7/4 + \varepsilon^2/8 (\ln 8/\varepsilon + 1/3) \right], \quad (2)$$

where μ_0 is the magnetic permeability of free space, $\varepsilon = th/(2R_e)$, th is the thickness of a mashed layer of micro-object (in the particular case, $th = 13 \mu\text{m}$).

Accounting for the values of diameters of levitation and stabilization coils, 3D geometrical scheme of the actuator for the eddy current simulation can be build as shown in Fig. 8. The position of the coordinate frame $\{x_k\}$ ($k = 1, 2, 3$) with respect to the fixed frame $\{X_k\}$ ($k = 1, 2, 3$) is defined by the radius vector $\underline{r}_{cm} = [0 \ 0 \ h_l]^T$, where the levitation height, h_l is to be $84 \mu\text{m}$. Then, the position of the s -mesh element with respect to the coordinate frame $\{{}^{(j)}z_k\}$ ($k = 1, 2, 3$) assigned to the j -coil filament can be found as ${}^{(s,j)}\underline{r} = \underline{r}_{cm} + {}^{(s)}\underline{\rho} - {}^{(j)}\underline{r}_c$ or in a matrix form as

$${}^{(s,j)}\underline{r}^z = {}^{(j)}\underline{A}^{zX} \underline{r}_{cm}^X + {}^{(j)}\underline{A}^{zx(s)} \underline{\rho}^x - {}^{(j)}\underline{A}^{zX(j)} \underline{r}_c^X, \quad (3)$$

where ${}^{(j)}\underline{A}^{zX} = {}^{(j)}\underline{A}^{zX} \left({}^{(j)}\underline{\phi}_c \right) = {}^{(j)}\underline{e}^z \cdot \underline{e}^X$ and ${}^{(j)}\underline{A}^{zx} = {}^{(j)}\underline{A}^{zX} \left({}^{(j)}\underline{\phi}_c \right) \underline{A}^{Xx}(\underline{\varphi}) = {}^{(j)}\underline{e}^z \cdot \underline{e}^x$ are the direction cosine matrices, $\underline{\varphi} = [0 \ 0 \ 0]$ is the vector of the angular generalized coordinates. Because

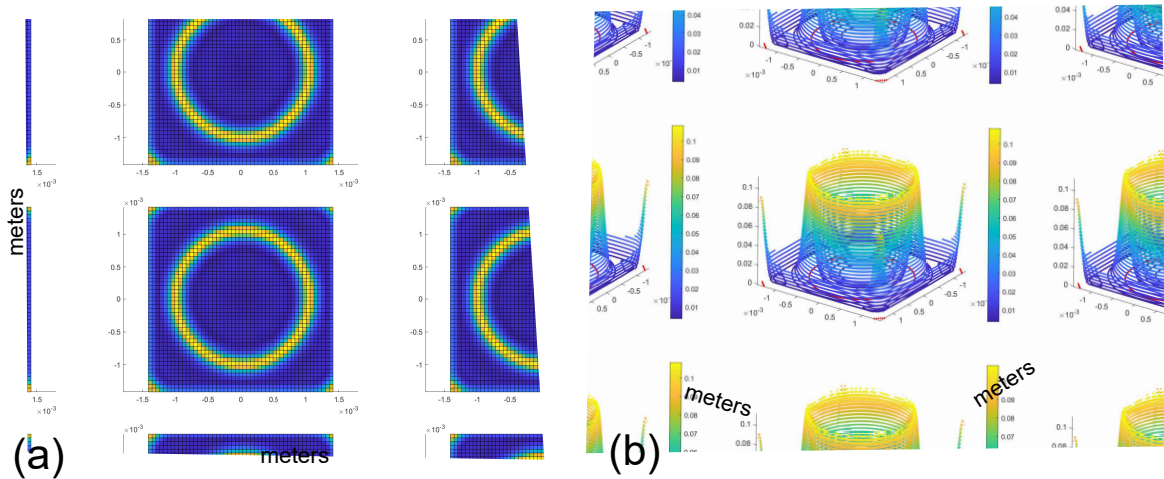


Figure 9. The distribution of magnitudes of eddy current with respect to unit vectors of e_1^x and e_2^x of the base e^x : (a) 2D plot; (b) 3D plot with intensity bar characterizes the value of dimensionless magnitude of the eddy current.

all angles are zero, hence ${}^{(j)}\underline{A}^{zx} = {}^{(j)}\underline{A}^{zX} = \underline{E}$, where \underline{E} is the (3×3) unit matrix. Since the coils are represented by the circular filaments and using the radius vector ${}^{(s,j)}\underline{r}$, the mutual inductance between the j -coil and s -meshed element can be calculated directly by the formula presented in [26]. Thereby, the the (2500×32) matrix \underline{M}_c of mutual inductance between coils and finite elements can be formed. The induced eddy current in each circular element is a solution of the following matrix equation

$$\underline{I} = \underline{L}^{-1} \underline{M}_c \underline{I}_c \quad (4)$$

where \underline{I} is the (2500×1) matrix of eddy currents and $\underline{I}_c = [I_{c1} I_{c2} \dots I_{cN}]^T$ is the given (32×1) matrix of currents in coils.

It is convenient to present the result of calculation in the dimensionless form. For this reason, the dimensionless currents in the levitation coil and stabilization one are introduced by dividing currents on the amplitude of the current in the levitation coil. Since the amplitudes of the current in both coil are the same. Hence, the input current in the levitation coil filaments is to be one, while in the stabilization coil filaments to be minus one (because of the 180° phase shift). Now, the induced eddy current in dimensionless values can be calculated [24]. The results of calculation are shown in Fig. 9. Fig. 9(a) shows the 2D plot of the distribution of magnitudes of eddy current along the area of the surface of the PM. While Fig. 9(b) shows the 3D plot. The intensity of the color shown by the bar characterizes the value of dimensionless magnitude of the eddy current. As it was expected, analysis of Fig. 9 depicts that maximum magnitudes of eddy current are concentrated along the edge of the PM and in its central part along the circle having the same diameter as the levitation coil. It is Worth noting that the obtained distribution of the eddy current within the square shaped PM is similar to one obtained by Lu in work [27] for the two coil design and the levitated disc shape PM.

3.2. Levitation force

Knowing the law of distribution of eddy current, the levitation dimensionless force can be calculated by using the following equation [24]:

$$F_m(\lambda) = \sum_{s=1}^n \sum_{j=1}^N \eta_{sj} \frac{\partial \overline{M}_{sj}(\bar{x}_1, \bar{x}_2, (1 + \lambda\kappa)\chi)}{\partial \lambda}, \quad (5)$$

where $\lambda = q_3/h_1$ is the dimensionless displacement along the X_3 axis, which is characterized by the generalized coordinate q_3 , $\eta_{sj} = \bar{I}_s \bar{I}_{cj} \sqrt{\bar{R}_{cj}}/\chi$, $\bar{I}_s = I_s/I_{c1}$ and $\bar{I}_{cj} = I_{cj}/I_{c1}$ are the dimensionless

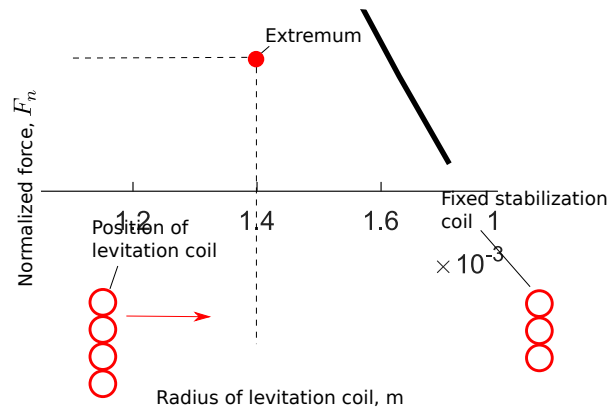


Figure 10. The normalized levitation force F_n vs a radius of levitation coil for the square shaped proof mass with a side length of 2.8 mm: the extremum of levitation force corresponding to a 1.0 mm radius of levitation coil is equal to 1.2.

currents, $\bar{R}_{cj} = R_{cj}/R_{c1}$, R_{c1} is the radius of the first winding of the levitation coil, $\chi = h_l/R_e$ is the scaling factor, $\partial\bar{M}_{sj}/\partial\lambda$ is the derivative of dimensionless mutual inductance with respect to λ .

The derivative of dimensionless mutual inductance is defined as follows:

$$\bar{M}_{sj} = \frac{1}{\pi} \int_0^{2\pi} \frac{1 + \bar{x}_1 \cdot \cos \varphi + \bar{x}_2 \cdot \sin \varphi}{\bar{\rho}^{1.5}} \frac{\Psi(k)}{k} d\varphi, \quad (6)$$

where

$$\bar{\rho} = \sqrt{1 + 2(\bar{x}_1 \cdot \cos \varphi + \bar{x}_2 \cdot \sin \varphi) + \bar{x}_1^2 + \bar{x}_2^2}; \quad (7)$$

$$\Psi(k) = \left(1 - \frac{k^2}{2}\right) K(k) - E(k); \quad (8)$$

$$k^2 = \frac{4v_j\bar{\rho}}{(v_j\bar{\rho} + 1)^2 + v_j^2\bar{x}_3^2}, \quad (9)$$

where $v_j = R_e/R_{cj}$, R_{cj} is the radius of the j -coil filament, \bar{x}_1 , \bar{x}_2 and \bar{x}_3 are the components of the radius vector \mathbf{r} in base \mathbf{e}^z (see Eq. (3)), which are defined in dimensionless form as $\bar{x}_1 = x_1/R_e$, $\bar{x}_2 = x_2/R_e$ and $\bar{x}_3 = x_3/R_e$.

The derivative of dimensionless mutual inductance with respect to \bar{x}_3 is

$$\frac{\partial\bar{M}_{sj}}{\partial\bar{x}_3} = \frac{1}{\pi} \int_0^{2\pi} \frac{1 + \bar{x}_1 \cdot \cos \varphi + \bar{x}_2 \cdot \sin \varphi}{\bar{\rho}^{1.5}} \Phi(k) d\varphi, \quad (10)$$

where

$$\Phi(k) = \frac{d}{d\bar{x}_3} \frac{\Psi(k)}{k} = \frac{1}{k^2} \left(\frac{2 - k^2}{2(1 - k^2)} E(k) - K(k) \right) \frac{dk}{d\bar{x}_3}, \quad (11)$$

$$\frac{dk}{d\bar{x}_3} = - \frac{v_j^2 \bar{x}_3 \sqrt{4v_j\bar{\rho}}}{\left((1 + v_j\bar{\rho})^2 + v_j^2 \bar{x}_3^2 \right)^{3/2}}. \quad (12)$$

Substituting $\bar{x}_3 = \lambda\chi$ into Eq. (10), the desired equation for the derivative of dimensionless mutual inductance with respect to λ is derived.

Noting that if a diameter of the levitation coil is equal to zero ($d_l = 0$), the levitation force is disappeared. But if a diameter the levitation coil is the same as the stabilization coil ($d_l = d_s$), the levitation force has the minimum value due to the minimization of the magnetic flux generated by both coils. Hence, between these two limit points can be found a particular value of a diameter of the

levitation coil, under which the levitation force has its maximum value. To show this, the levitation force is calculated from a following range of radius the levitation coil, which is 0.5 mm to 1.8 mm for the square shaped proof mass with a side length of 2.8 mm and a levitation height of 84 μm . The result of calculation is shown in Fig. 10. The levitation force is presented in the normalized value $F_n = F_m(1)/F_{m0}(1)$, where $F_{m0}(1)$ is calculated for a 0.5 mm radius of the levitation coil. The analysis of Fig. 10 shows the existence of extremum of levitation force and, as a result, confirms the fact that the fabricated two coil design is the optimum for levitation of the square shape PM with a side length of 2.8 mm.

4. Conclusions

In this paper, we developed the control circuit for application to inductive levitation micro-actuators. The developed control circuit was fabricated on a four layer PCB board having a size of $60 \times 60 \times 25$ mm, which is comparable with size of levitation micro-actuators. The developed circuit is able to generate AC current with squared shape in a range of frequency from 8 to 43 MHz and with peak-to-peak amplitude up to 420 mA. The fabricated device of ILMA composed of two solenoidal coil design including levitation and stabilisation coil, having 2 mm and 3.8 mm in diameters, respectively, was excited by using the developed control circuit. We demonstrated successful levitation of disc shaped PM of diameters of 2.8 mm and 3.2 mm and, for the first time, square shaped PM of a side length of 2.8 mm at excitation frequency of 10 MHz. This fact confirmed the efficiency of the proposed circuit design and its compatibility with micro-actuation system.

Applying a quasi-finite element method, we simulated the distribution of induced eddy current within the square shaped PM of a side length of 2.8 mm, which showed that maximum magnitudes of eddy current are concentrated along the edge of the PM and in its central part along the circle having the same diameter as the levitation coil. The numerical analysis of the force interaction between the coils and the levitated proof mass along the vertical direction shows the existence of extremum of levitation force and, as a result, confirms the fact that the fabricated two coil design provides the optimum coil design for levitation of the square shape PM with a side length of 2.8 mm.

5. Materials

The printed circuit board (PCB) was manufactured by Beta Layout GmbH (Aarbergen, Germany). The basic electronic components such as capacitors, diodes, resistors, switches, etc were acquired in house. The main electronic components for the control circuit are listed below:

- Voltage regulator, chip 78L05 IC1 (National Semiconductors, Danbury, United States of America) [28];
- Frequency oscillator, chip LTC6905 (Linear Technology, Milpitas, United States of America) [29];
- Frequency divider, chip D-FF-IC3 (Texas Instruments, Dalas, United States of America) [30];
- High-power output current feedback amplifier THS3491 (Texas Instruments, Dalas, United States of America) [31].

Author Contributions:

Conceptualization J.V. and K.P., writing–review and editing, K.P.; writing–original draft preparation, methodology and visualization V.V.; investigation V.V. and S.W.; validation, J.V.; resources, K.P. and M.K.; supervision, K.P.; M.K. and J.K.; project administration, K.P. and M.K.; funding acquisition, K.P.

Funding: This research was funded by the German Research Foundation grant number KO 1883/26-1.

Conflicts of Interest: The authors declare no conflict of interest.

Abbreviations

The following abbreviations are used in this manuscript:

ILMA	Inductive Levitation Micro-Actuator
PM	Proof Mass
MLMA	Magnetic Levitation Micro-Actuator
ELMA	Electric Levitation Micro-Actuator

References

- Jin, J.; Yih, T.C.; Higuchi, T.; Jeon, J.U. Direct electrostatic levitation and propulsion of silicon wafer. *IEEE Transactions on Industry Applications* **1998**, *34*, 975–984. doi:10.1109/28.720437.
- Murakoshi, T.; Endo, Y.; Fukatsu, K.; Nakamura, S.; Esashi, M. Electrostatically levitated ring-shaped rotational gyro/accelerometer. *Jpn. J. Appl. Phys* **2003**, *42*, 2468–2472.
- Han, F.T.; Liu, Y.F.; Wang, L.; Ma, G.Y. Micromachined electrostatically suspended gyroscope with a spinning ring-shaped rotor. *Journal of Micromechanics and Microengineering* **2012**, *22*, 105032.
- Poletkin, K.V.; Asadollahbaik, A.; Kampmann, R.; Korvink, J.G. Levitating Micro-Actuators: A Review. *Actuators* **2018**, *7*. doi:10.3390/act7020017.
- Coombs, T.A.; Samad, I.; Ruiz-Alonso, D.; Tadinada, K. Superconducting micro-bearings. *IEEE Transactions on Applied Superconductivity* **2005**, *15*, 2312–2315. doi:10.1109/TASC.2005.849640.
- Lu, Z.; Poletkin, K.; den Hartogh, B.; Wallrabe, U.; Badilita, V. 3D micro-machined inductive contactless suspension: Testing and modeling. *Sensors and Actuators A: Physical* **2014**, *220*, 134 – 143. doi:https://doi.org/10.1016/j.sna.2014.09.017.
- Poletkin, K.V.; Lu, Z.; Moazenzadeh, A.; Mariappan, S.G.; Korvink, J.G.; Wallrabe, U.; Badilita, V. Polymer Magnetic Composite Core Boosts Performance of Three-Dimensional Micromachined Inductive Contactless Suspension. *IEEE Magnetics Letters* **2016**, *7*, 1–3. doi:10.1109/LMAG.2016.2612181.
- Shearwood, C.; Williams, C.B.; Mellor, P.H.; Chang, K.Y.; Woodhead, J. Electro-magnetically levitated micro-discs. IEE Colloquium on Microengineering Applications in Optoelectronics, 1996, pp. 6/1–6/3. doi:10.1049/ic:19960241.
- Xiao, Q.; Wang, Y.; Dricot, S.; Kraft, M. Design and experiment of an electromagnetic levitation system for a micro mirror. *Microsystem Technologies* **2019**, *25*, 3119–3128.
- Shearwood, C.; Ho, K.Y.; Williams, C.B.; Gong, H. Development of a levitated micromotor for application as a gyroscope. *Sensor. Actuat. A-Phys.* **2000**, *83*, 85–92.
- Su, Y.; Xiao, Z.; Ye, Z.; Takahata, K. Micromachined Graphite Rotor Based on Diamagnetic Levitation. *IEEE Electron Device Letters* **2015**, *36*, 393–395. doi:10.1109/LED.2015.2399493.
- Garmire, D.; Choo, H.; Kant, R.; Govindjee, S.; Sequin, C.; Muller, R.; Demmel, J. Diamagnetically levitated MEMS accelerometers. Solid-State Sensors, Actuators and Microsystems Conference, 2007. TRANSDUCERS 2007. International. IEEE, 2007, pp. 1203–1206.
- Dieppedale, C.; Desloges, B.; Rostaing, H.; Delamare, J.; Cugat, O.; Meunier-Carus, J. Magnetic bistable micro-actuator with integrated permanent magnets. Proc. IEEE Sensors, 2004, Vol. 1, pp. 493–496.
- Abadie, J.; Piat, E.; Oster, S.; Boukallel, M. Modeling and experimentation of a passive low frequency nanoforce sensor based on diamagnetic levitation. *Sensor. Actuat. A-Phys.* **2012**, *173*, 227–237.
- Poletkin, K.V.; Lu, Z.; Wallrabe, U.; Korvink, J.G.; Badilita, V. A qualitative technique to study stability and dynamics of micro-machined inductive contactless suspensions. 2017 19th International Conference on Solid-State Sensors, Actuators and Microsystems (TRANSDUCERS), 2017, pp. 528–531. doi:10.1109/TRANSDUCERS.2017.7994102.
- Sari, I.; Kraft, M. A MEMS Linear Accelerator for Levitated Micro-objects. *Sensor. Actuat. A-Phys.* **2015**, *222*, 15–23.
- Poletkin, K.; Lu, Z.; Wallrabe, U.; Badilita, V. A New Hybrid Micromachined Contactless Suspension With Linear and Angular Positioning and Adjustable Dynamics. *Journal of Microelectromechanical Systems* **2015**, *24*, 1248–1250. doi:10.1109/JMEMS.2015.2469211.
- Xu, Y.; Cui, Q.; Kan, R.; Bleuler, H.; Zhou, J. Realization of a Diamagnetically Levitating Rotor Driven by Electrostatic Field. *IEEE/ASME Transactions on Mechatronics* **2017**, *22*, 2387–2391. doi:10.1109/TMECH.2017.2718102.
- Xu, Y.; Zhou, J.; Bleuler, H.; Kan, R. Passive diamagnetic contactless suspension rotor with electrostatic glass motor. *Micro & Nano Letters* **2019**, *14*, 1056–1059.

20. Chen, X.; Keskekler, A.; Alijani, F.; Steeneken, P.G. Rigid body dynamics of diamagnetically levitating graphite resonators. *Applied Physics Letters* **2020**, *116*, 243505, [<https://doi.org/10.1063/5.0009604>]. doi:10.1063/5.0009604.
21. Kratt, K.; Badilita, V.; Burger, T.; Korvink, J.; Wallrabe, U. A fully MEMS-compatible process for 3D high aspect ratio micro coils obtained with an automatic wire bonder. *Journal of Micromechanics and Microengineering* **2010**, *20*, 015021.
22. Lu, Z.; Poletkin, K.; Wallrabe, U.; Badilita, V. Performance Characterization of Micromachined Inductive Suspensions Based on 3D Wire-Bonded Microcoils. *Micromachines* **2014**, *5*, 1469–1484. doi:10.3390/mi5041469.
23. Poletkin, K.; Lu, Z.; Wallrabe, U.; Korvink, J.; Badilita, V. Stable dynamics of micro-machined inductive contactless suspensions. *International Journal of Mechanical Sciences* **2017**, *131-132*, 753 – 766. doi:<https://doi.org/10.1016/j.ijmecsci.2017.08.016>.
24. Poletkin, K. Static Pull-in Behavior of Hybrid Levitation Micro-Actuators: Simulation, Modelling and Experimental Study. *IEEE/ASME Transactions on Mechatronics* **2020**, pp. 1–1.
25. Poletkin, K.V. *Levitation Micro-Systems: Applications to Sensors and Actuators*, 1 ed.; Springer International Publishing: p. 145. doi:10.1007/978-3-030-58908-0.
26. Poletkin, K.V.; Korvink, J.G. Efficient calculation of the mutual inductance of arbitrarily oriented circular filaments via a generalisation of the Kalantarov-Zeitlin method. *Journal of Magnetism and Magnetic Materials* **2019**, *483*, 10–20. doi:<https://doi.org/10.1016/j.jmmm.2019.03.078>.
27. Lu, Z.; Jia, F.; Korvink, J.; Wallrabe, U.; Badilita, V. Design optimization of an electromagnetic microlevitation System based on copper wirebonded coils. *2012 Power MEMS*, 2012; pp. 363 – 366.
28. National Semiconductors. Data sheet: LM78LXX Series3-Terminal Positive Regulators, available on: <http://users.ece.utexas.edu/~valvano/Datasheets/LM78L05.pdf>, accessed in: 09.10.2020.
29. Linear Technologies. Data sheet: LTC6905 - 17 MHz to 170 MHz Resistor Set SOT-23 Oscillator, available on: <https://www.analog.com/media/en/technical-documentation/data-sheets/6905fd.pdf>, accessed in: 09.10.2020.
30. Texas Instruments. Data sheet: D-FFIC3 - SN74LVC1G74 Single Positive-Edge-Triggered D-Type Flip-Flop with Clear and Preset, available on: <https://www.ti.com/lit/ds/symlink/sn74lvc1g74.pdf>, accessed in: 09.10.2020.
31. Texas Instruments. Data sheet: THS3491 - 900-MHz, 500-mA High-Power Output Current Feedback Amplifier, available on: <https://www.ti.com/lit/ds/symlink/th3491.pdf>, accessed in: 09.10.2020.

© 2020 by the authors. Submitted to *Actuators* for possible open access publication under the terms and conditions of the Creative Commons Attribution (CC BY) license (<http://creativecommons.org/licenses/by/4.0/>).